Phase space transport in the interaction between shocks and plasma turbulence

Domenico Trotta[a,1], Francesco Valentini[a], David Burgess[b], and Sergio Servidio[a]

[a]Dipartimento di Fisica, Università della Calabria, I-87036 Cosenza, Italy; and [b]School of Physics and Astronomy, Queen Mary University of London, London E1 4NS, United Kingdom

Edited by Gary P. Zank, University of Alabama in Huntsville, Huntsville, AL, and approved April 14, 2021 (received for review December 30, 2020)

The interaction of collisionless shocks with fully developed plasma turbulence is numerically investigated. Hybrid kinetic simulations, where a turbulent jet is slammed against an oblique shock, are employed to address the role of upstream turbulence on plasma transport. A technique, using coarse graining of the Vlasov equation, is proposed, showing that the particle transport strongly depends on upstream turbulence properties, such as strength and coherency. These results might be relevant for the understanding of acceleration and heating processes in space plasmas.

collisionless shocks | plasma turbulence | particle acceleration | particle transport

A turbulent plasma wind flows from the sun and permeates the heliosphere, encountering several magnetic obstacles, leading to shocks that continuously interact with the incoming complex solar wind—a scenario that becomes a prototype for understanding many other systems characterized by the presence of shocks. Despite decades of research, the interaction of shocks with plasma turbulence and the subsequent energetic particle production still remain poorly understood (1, 2). Shocks are well-known efficient, natural particle accelerators (3) and have been modeled in a number of theories (4–8). Less understood is the interaction of shocks and turbulence that characterizes spectacular high-energy events, as in supernovae explosions propagating through the interstellar turbulent medium, as in the case of coronal mass ejections that stream through the turbulent solar wind, and as for the complex Earth's bow shock environment. In many of the above examples, oblique shocks are known to generate coherent field-aligned beams (FABs), as observed at Earth's bow shock (9). FABs are an important source of free energy throughout the interplanetary medium (10). Turbulence-generated coherent structures and waves might interact with the shock discontinuity, in an interplay that is likely to play a pivotal role in particle acceleration and plasma heating (11–13).

Turbulence is populated by a variety of structures that can work effectively as particle "traps" and "corridors" that either hinder or enable their motion (14) and represents another crucial source of accelerated particles (15–18). An example of such an energization process has been observed in the patterns of local reconnection that develop in turbulence (19, 20). In order to understand such mechanisms, the transport properties need to be explored in the plasma phase space (21).

Due to the difference between the spatial and temporal scales involved in accelerating particles, shocks and turbulence are often considered theoretically in isolation rather than together. However, fundamental studies have suggested that these are inextricably linked: Shocks are likely to propagate in turbulent media, and turbulence is responsible for changing fundamental aspects of shock transitions (22–27). Inspired by these studies, here we quantitatively explore the intimate relation between these two phenomena.

Simulations of Shocks Propagating through Turbulent Media

Hybrid Vlasov–Maxwell particle-in-cell (PIC) simulations have been employed in two dimensions (2D), where a turbulent jet, generated via compressible magnetohydrodynamic (MHD) simulations, is released upstream against a supercritical shock. We investigate the shock–turbulence interaction and its role on particle transport using both Lagrangian and Eulerian approaches. We present a technique to investigate the transport processes at play based on coarse-grained techniques, typical of fluid dynamics, accompanied by velocity space integration, typical of energetic particle transport models.

The methodology is based on two stages. First, fully developed, decaying turbulence is generated by MHD simulations in 2.5 dimensions (28). Four simulations were performed with different levels of turbulence fluctuations, namely $\delta B/B_0 = 0.0, 0.4, 0.8, 2.1$, where δB is the rms of fluctuations, B_0 is the mean field at $\theta_{Bn} = 45^\circ$ in the x–y plane, and θ_{Bn} represents the angle between the upstream magnetic field and the shock normal. When the rms of the out-of-plane current density J_z reaches its peak (29), turbulence might be considered as fully developed, and coherent structures form.

The second (main) step consists of using the MHD output, with adequate windowing, as an upstream condition for a kinetic, hybrid PIC simulation of a supercritical shock performed through the HYbrid Plasma SImulation (HYPSI) code (30). In this main stage, the Vlasov–Maxwell equations are solved with fluid electrons and kinetic ions, and the injection method for the shock generation is used (31), where the shock propagates in the negative x direction, while the turbulent pattern moves oppositely, in the upstream region.

In the MHD simulations, typical Alfvén units have been specified for a periodic box. In the hybrid PIC simulations, distances are normalized to the ion inertial length $d_i \equiv c/\omega_{pi}$ (where c

Significance

Shocks and turbulence are spectacular, ubiquitous phenomena. In this work, we investigate, by kinetic simulations, the interaction between a supercritical shock and fully developed plasma turbulence. We demonstrate how turbulence dramatically changes the phase space transport due to a complex interaction. Two main findings are presented: 1) a paradigm for modeling the shocks, including a natural interaction with surrounding turbulence, and 2) an analysis method, based on coarse-grained kinetic equations, able to characterize (and simplify) the transport processes. These results are relevant for a variety of systems, ranging from the Earth's bow shock interacting with solar wind turbulence to supernovae explosions propagating through the interstellar turbulent medium.

Author contributions: D.T., F.V., and S.S. designed research; D.T. and F.V. performed research; D.T., F.V., D.B., and S.S. contributed new reagents/analytic tools; D.T. and S.S. analyzed data; S.S. derived the theory; F.V. helped with writing the paper; and D.T. and S.S. wrote the paper.

The authors declare no competing interest.

This article is a PNAS Direct Submission.

[1]To whom correspondence may be addressed. Email: domenico.trotta@unical.it.

Published May 18, 2021.

is the speed of light and ω_{pi} is the proton's plasma frequency), times are normalized to the inverse cyclotron frequency $\Omega_{ci}{}^{-1}$ and velocity is normalized to the Alfvén speed v_A. All the quantities mentioned above are referred to their unperturbed upstream state. Magnetic field and density are also normalized to their unperturbed, upstream values (namely, B_o and n_0). An upstream flow with $V_{\rm in} = 3.5 v_A$ has been chosen, resulting in an Alfvénic Mach number of the shock $M_A = 5.5$. The upstream ion distribution function is an isotropic Maxwellian and the ion $\beta_i = 1$, as in the MHD simulation. The simulation domain is 256 d_i × 256 d_i, with a grid size $\Delta x = \Delta y = 0.5$ d_i and a particle time step $\Delta t_{pa} = 0.01\ \Omega_{ci}^{-1}$. The number of particles specified per cell is large, always greater than 500 (upstream), in order to keep the statistical noise at a very low level.

This technique represents a realistic step forward with respect to "laminar" injection and is different from other perturbation methods, where uncorrelated random noise or a prescribed spectrum of fluctuations is introduced upstream (24, 25). Here, turbulence consists of a fully developed spectrum of fluctuations, with a large variety of coherent structures and waves, which are crucial for the transport properties, as predicted by important theoretical works (12, 32).

Fig. 1 *A*–*C* shows an overview of the perturbed simulations, where we report the 2D color maps of the magnetic field intensity B. The shock front is interacting with the perturbed upstream medium, and there is a net change of topology for increasing turbulence level. Fig. 1*D* shows the upstream energy spectra for all cases. When $\delta B/B_0 = 0$ (unperturbed case), the spectrum shows the Maxwellian inflow population together with a narrow beam of accelerated particles, namely the FAB. Turbulence manifests in three ways. First, for higher upstream turbulence strength, particles achieve higher energies. Second, the high-energy FAB shifts and spreads for increasing $\delta B/B_0$, suggesting that some mechanism of beam "decoherence" is at play. The third effect is the production of very low-energy particles, evidently related to a process of particle deceleration and trapping. These features are possibly due to field–particle interactions, where typical turbulence patterns act as spreaders or transport barriers (14, 20, 33). These changes in energy spectra are intimately related to phase space transport and diffusion, as discussed later.

Intermittency is a peculiar property of inertial-range turbulence that manifests as a deviation from the classical Kolmogorov's self-similarity (34). In particular, the dissipation rate is highly inhomogeneous, both in fluids and plasmas. Local patterns of non-Gaussian statistics manifest as current sheets, where usually reconnection takes place (e.g., ref. 35). We first inspect the classical spectral behavior for all of the runs performed, as reported in Fig. 2*A*. For simplicity, we computed the power spectra of the magnetic field fluctuations in the periodic direction (y), integrated over the nominal shock normal direction (x) in the upstream region (magenta boxes in Fig. 1). As can be seen, spectral laws typical of plasma turbulence are recovered.

It is important, at this point, to measure the degree of coherency with a classical intermittency analysis (e.g., refs. 29 and 36). A simple surrogate measurement of intermittency is given by the magnetic field increments at the smallest scales (37). In this regard, in Fig. 2*B*, we show the probability density functions (PDFs) of the current density J_z (normalized to its rms value σ_{J_z}). The classical non-Gaussian tails are observed as the turbulence strength increases. In Fig. 2 *B*, *Inset*, a quantitative measurement of the intermittency level is given by the kurtosis, which is three for typical uncorrelated noise and more than three when coherent structures are present. The analysis reveals the absence of intermittency in the unperturbed case, while it rises with turbulence amplitude. Finally, to give a general picture of the coherency patterns, we show the out-of-plane magnetic potential contours on top of the magnetic field magnitude, together with the extreme values of the current (Fig. 2*C*),

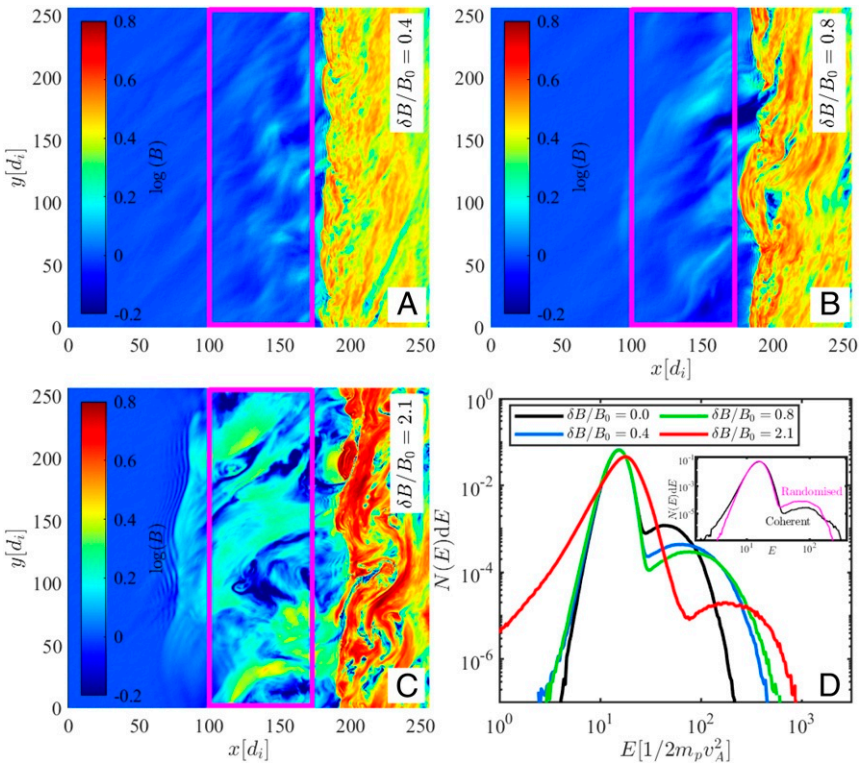

Fig. 1. (*A*) The 2D color maps of magnetic field magnitude *B* for the perturbed shocks and with different upstream turbulence strengths (*A*–*C*). (*D*) Upstream energy spectra collected in the regions highlighted by the magenta boxes. *Inset* shows a comparison of simulation using coherent and incoherent initial conditions for the $\delta B/B_0 = 0.8$ case.

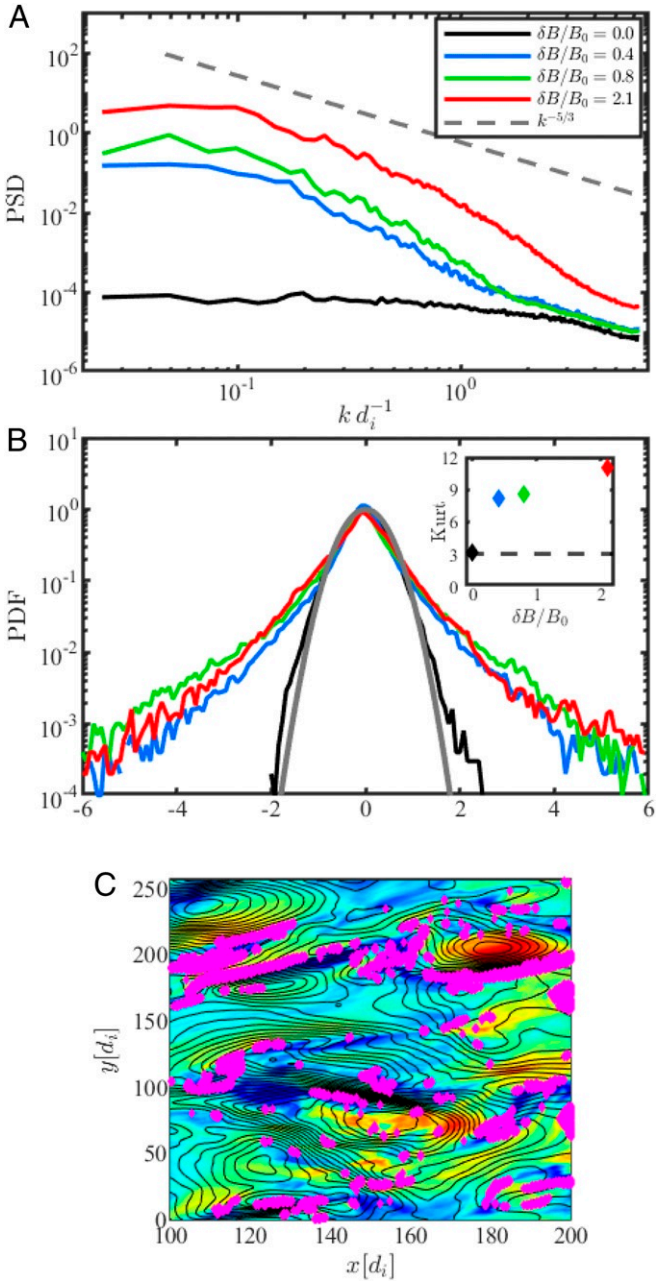

Fig. 2. Properties of upstream turbulence during its interaction with the shock. (*A*) Magnetic field power spectral density (PSD) collected upstream in the (magenta) boxes shown in Fig. 1 for all of the cases. A Kolmogorov spectrum ($k^{-5/3}$) is shown for comparison (dashed line). (*B*) PDFs of standardized current density J_z/σ_{J_z} (colors are the same as in *A*) in comparison with a Gaussian distribution (gray line). (*Inset*) Kurtosis as a function of turbulence strength. (*C*) Zoom of the upstream region for the strongly perturbed ($\delta B/B_0 = 2.1$) case, with the magnetic field intensity (shaded contours) and out-of-plane magnetic potential (black lines). The (magenta) dots represent extreme values of J_z/σ_{J_z}.

that are localized along with the current sheets in between turbulent islands. These patterns might be crucial for phase space transport.

In order to understand the importance of coherency, we performed a simulation where we used the same MHD perturbation (i.e., with the same spectrum) but randomized the phases. In this way, all of the coherent structures interactions are lost. In the random case, phase space diffusion is less efficient, as can be seen from Fig. 1 *D*, *Inset*, where we compare the upstream energy spectra for both cases.

In order to extract more details about the transport processes, we reconstruct the upstream particles velocity distribution functions (VDFs), fundamental for an Eulerian approach (32, 38–40). In Fig. 3, we report examples of such VDFs, integrated along v_z, in the $v_x - v_y$ velocity space, for all of the simulations. In the unperturbed case, the inflow population and the reflected FAB are well separated. When upstream turbulence is present, the separation between the two populations is much less sharp. A "distortion" of the inflow population is observed, due to the turbulent plasma heating at the shock front, particularly prominent for the most turbulent case. Following in sequence the perturbation amplitudes, it is evident that turbulence smooths and diffuses the two particle populations that spread toward both high and lower energies, as reported in Fig. 1*D*. It is now natural to ask how particles behave in the velocity subspace. In Fig. 3, some typical phase space trajectories of energetic protons, superimposed on the VDFs, are reported. While in low-turbulence cases, the particles remain confined in sectors of the velocity space, they can break down transport barriers thanks to higher turbulence levels. On this observation, we base our method, described below.

The Coarse-Graining Technique for Phase Space Transport

The premise is that the shock–turbulence interaction is a multiscale process characterized by a variety of "lengths," both in physical and velocity subspace. It is natural to approach such multidimensional complexity via coarse-graining and filtering techniques, successfully used for decades in fluid dynamics (41). Recent progress on this front was made also in plasma kinetic equations (42), as well as in fluid plasma modeling (43).

The idea is to identify phase space sectors where dispersion/trapping and acceleration/deceleration are at play. Our technique relies on a coarse graining of the Vlasov equation (42), combined with a computation of the reduced (coarse-grained) moments. In order to simplify our model at a basic level, we reduce it to a 2D-2V (i.e., two spatial dimensions and two dimensions in velocity space) description. By integrating along v_z, we define $F(x, y, v_x, v_y, t) = \int_{-\infty}^{+\infty} f(\mathbf{x}, \mathbf{v}, t)\mathrm{d}v_z$, where $f(\mathbf{x}, \mathbf{v}, t)$ is the ion VDF. This leads to

$$\partial_t F + \nabla \cdot (\mathbf{v}F) + \nabla_v \cdot (\mathbf{P}F) = 0, \qquad [1]$$

where $\mathbf{E}$ and $\mathbf{B}$ are the electric and magnetic fields, respectively, and the acceleration is given by $\mathbf{P}(\mathbf{x}, \mathbf{v}) = \mathbf{E} + \mathbf{v} \times \mathbf{B}$ on reduced 2D-2V phase space with coordinates (x, y, v_x, v_y). We concentrate on a coarse-grained Vlasov equation, by defining a scale-dependent, filtered distribution

$$\overline{F}_l(\mathbf{x}, \mathbf{v}, t) = \int_{-\infty}^{+\infty} f(\mathbf{x} + \mathbf{r}, \mathbf{v}, t)\, G_l(\mathbf{r})\, d^2 r, \qquad [2]$$

where $G_l(\mathbf{r})$ is a kernel that satisfies a series of properties, being nonnegative, normalized, centered, and rapidly approaching to zero for $r \to \infty$. In our case, we chose the simplest box-filter type that in the reduced 2D Cartesian coordinate system is given by $G_l(\mathbf{r}) = 1/l^2$ for $|r_x| < l/2$ and $|r_y| < l/2$ and equal to zero otherwise. By filtering Eq. **1**, it is easy to get

$$\partial_t \overline{F}_l + \nabla_l \cdot \left[\mathbf{v}\overline{F}_l\right] + \nabla_v \cdot \left[\overline{\mathbf{P}}_l \overline{F}_l\right] = \nabla_v \cdot \overline{\mathbf{Q}}_l, \qquad [3]$$

where $\overline{\mathbf{P}F}_l = \overline{\mathbf{P}}_l \overline{F}_l - \overline{\mathbf{Q}}_l$. The latter decomposition, typical of Reynolds-averaging techniques (44), introduces the "closure problem," related to the description of the subgrid modeling (45), equivalent to turbulent diffusion due to small-scale eddies.

In analogy with the Parker equation for energetic particle transport, we choose a typical speed w (and therefore, a typical

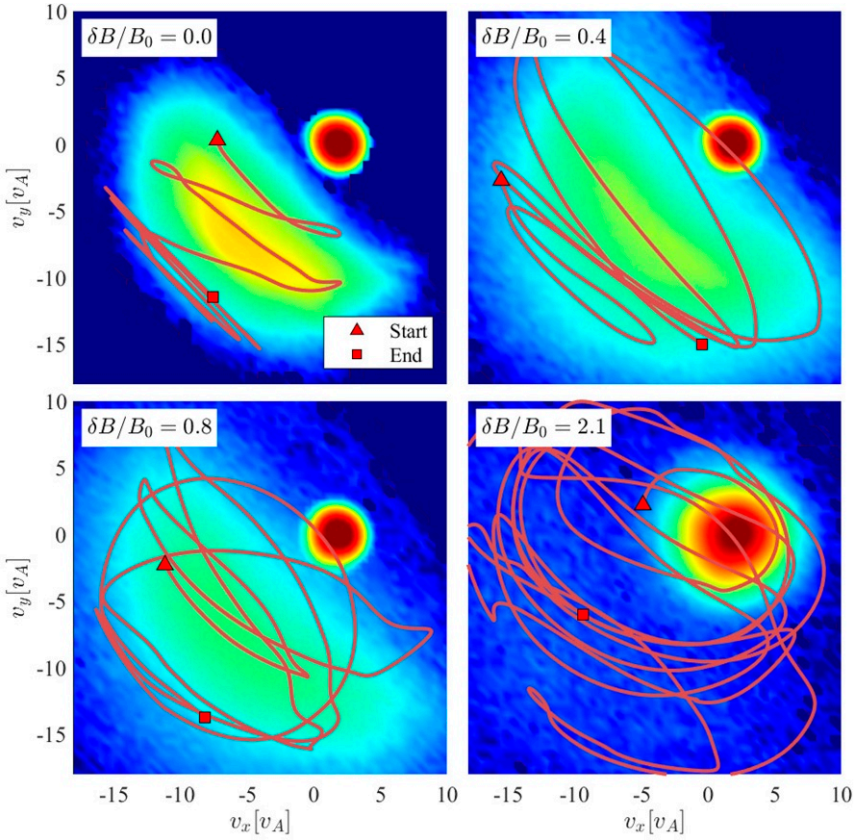

Fig. 3. Protons VDFs in the shock upstream (collected in the magenta boxes in Fig. 1) at different turbulence levels. Particles trajectories are reported from the beginning to the end of the shock–turbulence interaction.

energy) at which we integrate Eq. **3** (46). The zeroth-reduced moment (21, 47), namely the reduced particle density, becomes

$$\overline{N}_{l,w}(x,y,t) = \int d^2v \overline{F}_l(x,y,\mathbf{v},t)\, G_w(\mathbf{v}), \qquad [4]$$

where now $G_w(\mathbf{v})$ is a unitary kernel, different from zero only for $|\mathbf{v}| < w$, and $\overline{N}_{l,w}(x,y,t)$ is the thermal population, coarse grained in space at scale l. Applying $G_w(\mathbf{v})$ and integrating Eq. **3**, one gets

$$\partial_t \overline{N}_{l,w} + \nabla_l \cdot \left[\overline{N}_{l,w}\overline{\mathbf{V}}_{l,w}\right] + \int_{\gamma_w} \overline{F}_l \overline{\mathbf{P}}_l \cdot \hat{\mathbf{n}}\, d\gamma = \int_{\gamma_w} \overline{\mathbf{Q}}_l \cdot \hat{\mathbf{n}}\, d\gamma. \qquad [5]$$

The first term represents the time variation of the reduced density, the second term is responsible for spatial transport of particles over the coarse-grained space, while the third represents the flux across a circle γ_w of radius w. The right-hand side is the residual contribution from the subgrid scales. Interestingly, the velocity space propagation term of Eq. **5** is essentially due to the normal component of the electric field, while the magnetic part of $\overline{\mathbf{P}}_l$ is tangent to the surface, acting as a pitch-angle spreader (48). Eq. **5** results from the 2D divergence theorem in velocity space for plasmas for spatial integration at a length scale l and at a velocity cutoff w. The advantage of the model is to describe the large-scale patterns of acceleration and diffusion processes. A simple study of the sign of the fluxes provides unique information about spatial diffusion/clusterization and about energization/deceleration.

An example of this Eulerian approach to velocity space diffusion is shown in Fig. 4*A*, with a cartoon of our velocity space integration circle γ_w and its normal $\hat{\mathbf{n}}$. The spatial coarse

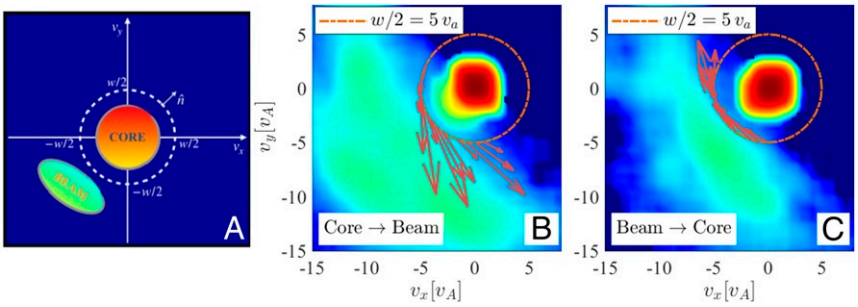

Fig. 4. (*A*) Sketch of typical particle distributions together with the integration surface γ_w (dashed white). (*B*) Upstream VDF in coarse-grained cell with positive flux $\int_\gamma \overline{F}_l \overline{\mathbf{P}}_l \cdot \hat{\mathbf{n}}\, d\gamma$. The vector $\overline{F}_l \overline{\mathbf{P}}_l$ is shown on the integration path (brown arrows). (*C*) The same as in *B* but in a region with negative flux.

graining l was chosen to be of $5d_i$, a value in the inertial range of the upstream turbulence spectrum. This is very important since the results obtained in this range are self-similar, typical of inertial-range coarse graining in fluids (49). We chose the w parameter to be $10v_A$, in such a way that the integration in velocity space is done between the core and the beam population. In Fig. 4 *B* and *C*, we represent $\overline{F}_l(\mathbf{x}, \mathbf{v}, t)$, at two different spatial cells, with positive (Fig. 4*B*) and negative (Fig. 4*C*) flux-integral $\int_{\gamma_w} \overline{F}_l \overline{\mathbf{P}}_l \cdot \hat{\mathbf{n}}\, d\gamma$. The VDFs are obtained from the intermediate turbulence case, $\delta B/B_0 = 0.8$, typical of solar wind conditions. A positive net flux through γ_w indicates an energization mechanism, where $\overline{N}_{l,w}$ diminishes. In the opposite case, a deceleration or cooling mechanism is at work, and the core gains particles (Fig. 4*C*).

At this point, a powerful aspect of our technique is to recognize phase space transport patterns in space. Following our governing Eq. **5**, we can identify regions of strong spatial dilatation (compression) and regions of strong acceleration (deceleration). In Fig. 5, we report this characterization of the phase space transport over a "pixelized" domain with resolution $l = 5d_i$. Fig. 5, *Top* shows a spatial transport overview. When the space transport is positive, thermal particles are escaping, evidently subject to the Alfvènic turbulence. On the other hand, when the spatial transport term is negative, plasma condensates. The overall picture for upstream velocity space transport is shown in Fig. 5,

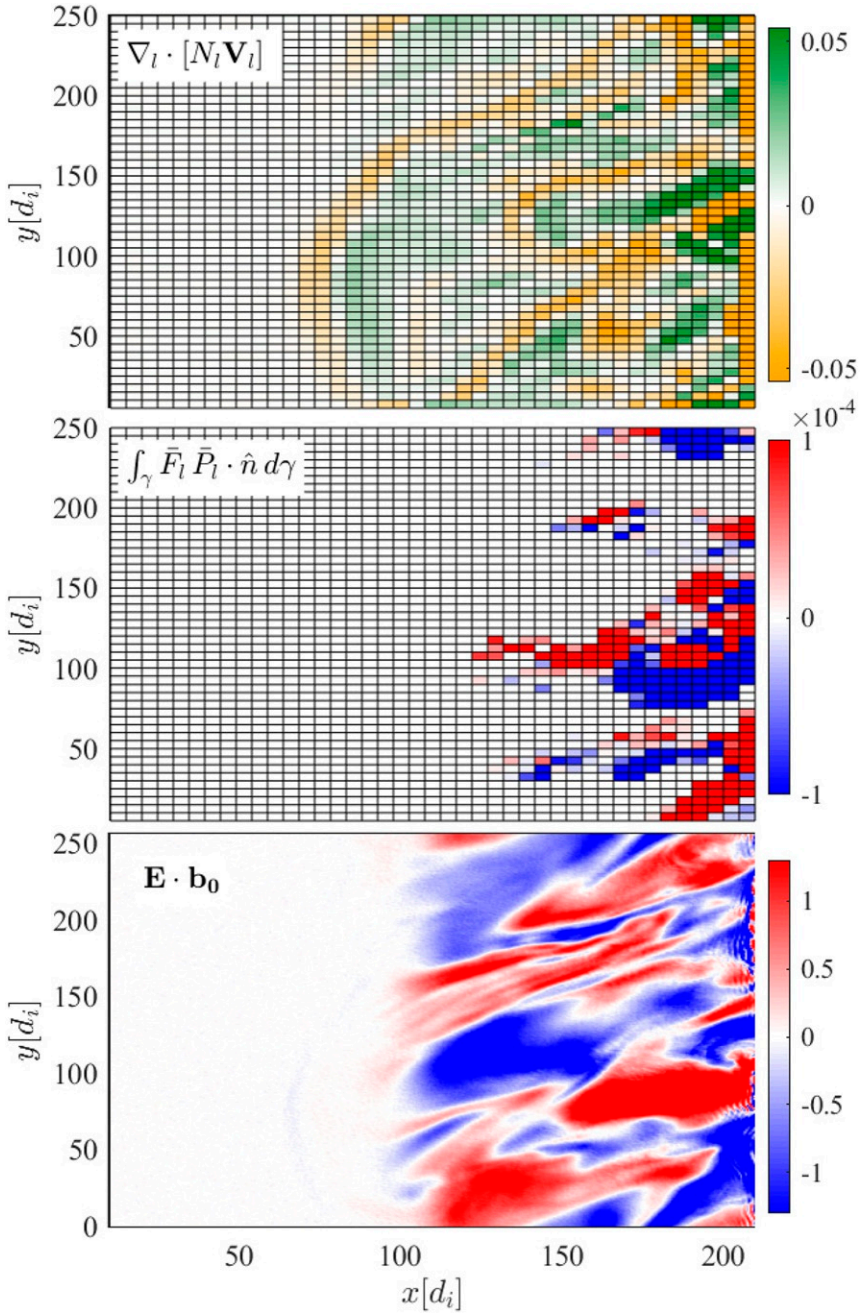

Fig. 5. Coarse-grained mosaic of the turbulence–shock interaction. Upstream spatial (*Top*) and velocity (*Middle*) transport terms, for moderate turbulence level, for coarse graining at $l = 5d_i$ and $w = 10v_A$. (*Bottom*) Parallel electric field.

Middle, being enhanced at the turbulence–shock boundary layer. As in the mechanism described in Fig. 4, a positive velocity transport ($\int_{\gamma_w} \overline{F}_l \overline{\mathbf{P}}_l \cdot \hat{\mathbf{n}}\, d\gamma$) indicates a net flux of the core population toward higher energies (beam population) and vice versa for very negative fluxes.

The enhanced velocity fluxes are evidently due to the interplay between particles and turbulent fields, where the $\mathbf{v} \times \mathbf{B}$ force acts as a pitch-angle spreader along the surface and the turbulent electric field locally enhances momentum diffusion, via local processes such as wave–particles interaction, linear and nonlinear Landau damping (50, 51), stochastic ion heating (52), and possible interaction with reconnection processes in the upstream turbulent layer (19, 40, 50). In order to establish such field–particle synergy and quantify the net transport across γ_w, we computed the electric field parallel to the mean field $\mathbf{B}_0$. As it can be seen from Fig. 5, there is a very good correlation between the parallel electric field $E_\parallel = \mathbf{E} \cdot \hat{\mathbf{b}}_0$ (which may be interpreted as the component of the turbulent motional electric field parallel to the background/guide field direction) and the velocity transport, especially for the most extreme values. We evaluated the correlation coefficient between the two terms, finding $C \simeq 0.7$. Large fluxes and parallel electric field are, as expected, anticorrelated, suggesting that any positive parallel electric field energizes particles.

In Fig. 6, we compare all of the numerical experiments by computing PDFs for both spatial and velocity space transport terms. Increasing upstream turbulence enhances the phase space transport, thus explaining the broader energies observed in Fig. 1. In the unperturbed case, the velocity space transport is very small; the core and beam population appear well separated when upstream perturbations are not present. In this scenario, particle acceleration happens only at the shock front. The efficiency of the mixing depends dramatically on the turbulence level, although even a small amount of turbulence is a very efficient diffusor.

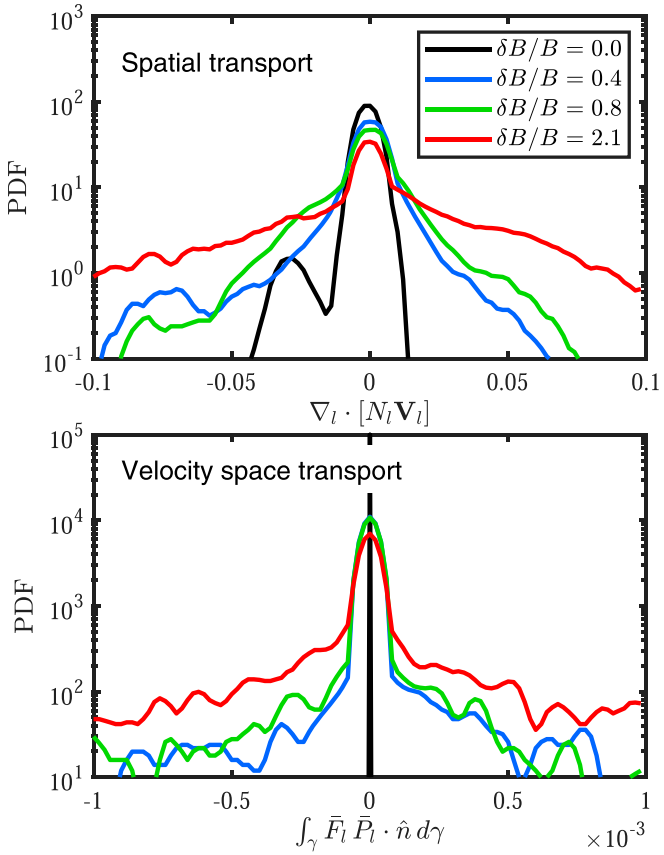

Fig. 6. PDFs of the spatial (*Upper*) and velocity space (*Lower*) fluxes for different upstream turbulence cases. The turbulence–shock interaction enhances the transport.

Furthermore, we suggest that the behavior observed in Fig. 6 could be linked to particles anomalous transport, induced by reflection at the shock front and the propagation in a turbulent medium. For instance, shock-reflected particles may show superdiffusive behavior (e.g., ref. 53), and coherent structures present in the up-/downstream of the shock provide excellent traps (or accelerators) for energetic particles (40).

The transmission of such coherent structures across the shock is crucial to achieve rapid particle energization away from the shock front (e.g., ref. 32). A detailed analysis of the transmission of coherent structures as well as an assessment of particle diffusion properties based on the reconstruction of trajectories will be the object of further studies.

Conclusions

In summary, the plasma behavior upstream of oblique shocks has been investigated in the presence of preexisting MHD-generated turbulence. A dramatic change of the plasma transport has been found, going from the unperturbed to the superturbulent case (Fig. 1), which has been investigated by using both Lagrangian and Eulerian approaches. From the Lagrangian point of view, particles can escape from their original population thanks to a "bridge" established by turbulence (Fig. 3). In order to understand such behavior, a Eulerian technique, based on the coarse graining of the Vlasov equation, has been proposed, where we combine spatial filtering, typical of hydrodynamics, with Parker-type transport equations, typical of cosmic ray physics (54). As it can be seen from Fig. 5, by averaging over inertial-range scales and by using a divergence theorem in velocity space, the turbulent upstream is made up of a "mosaic," where each piece of such puzzle is characterized from strong spatial dilation and condensation, thanks to the Alfvènic turbulent modulations. More interestingly, the v-space filtered flux is noticeably anticorrelated with the parallel electric field, suggesting the possibility of several field–particles interactions.

Whereas previous kinetic simulations either produce turbulence only self-consistently starting with a no background turbulence initial condition or prescribe background turbulence artificially as an initial condition, the simulations in this paper introduce background coherent turbulence initiated by MHD simulations. The simulations yielded interesting results, illustrating 1) how increasing the initial turbulence level and the presence of coherent structures ahead of a shock results in more efficient diffusive-like spreading of particles in both ordinary and velocity space and 2) how the turbulent electric field parallel to the background magnetic field plays an important part in particle velocity diffusion.

In this scenario, our analysis reveals that the level of turbulence intermittency, which increases simultaneously with its intensity, is crucial for the formation of accelerated/decelerated particle patterns—as predicted in previous seminal works (40), where eddies and coherent structures profoundly change the nature of the transport.

Our results also suggest that modifications to theories such as, for example, the diffusive shock acceleration theory are probably required when shocks propagate through turbulence, due to the strong changes in the (anomalous) transport behavior of particles and subsequently, on the injection stage to higher energies. These issues will be addressed in future works employing larger spatial/temporal simulation domains.

These results might have important consequences for the understanding of transport and heating processes in a variety of systems, ranging from the Earth's bow shock interacting with the

turbulent solar wind to more energetic, spectacular events such as supernova remnants (e.g., ref. 55).

In future works, we will extend the analysis to the full phase space and include the effect of kinetic electrons, with possible applications to in situ measurements (56, 57).

Data Availability. Simulation data have been deposited in Zenodo (DOI: 10.5281/zenodo.4590173).

ACKNOWLEDGMENTS. This work has received funding from the European Union's Horizon 2020 Research and Innovation Program Grant 776262 (Artificial Intelligence Data Analysis; http://www.aida-space.eu/).

1. A. M. Bykov, F. Vazza, J. A. Kropotina, K. P. Levenfish, F. B. S. Paerels, Shocks and nonthermal particles in clusters of galaxies. *Space Sci. Rev.* **215**, 14 (2019).
2. A. Lazarian *et al.*, Turbulence, magnetic reconnection in turbulent fluids and energetic particle acceleration. *Space Sci. Rev.* **173**, 557–622 (2012).
3. D. Burgess, M. Scholer, *Collisionless Shocks in Space Plasmas: Structure and Accelerated Particles* (Cambridge University Press, 2015).
4. W. I. Axford, E. Leer, G. Skadron, The acceleration of cosmic rays by shock waves. *Int. Cosmic Ray Conf.* **11**, 132–137 (1977).
5. A. R. Bell, The acceleration of cosmic rays in shock fronts. I.*Mon. Not. R. Astron. Soc.* **182**, 147–156 (1978).
6. G. F. Krymskii, A regular mechanism for the acceleration of charged particles on the front of a shock wave. *Akademiia Nauk SSSR Doklady* **234**, 1306–1308 (1977).
7. R. D. Blandford, J. P. Ostriker, Particle acceleration by astrophysical shocks. *ApJ Lett.* **221**, L29–L32 (1978).
8. T. Katou, T. Amano, Theory of stochastic shock drift acceleration for electrons in the shock transition region. *Acta Pathol. Jpn.* **874**, 119 (2019).
9. G. Paschmann, N. Sckopke, J. R. Asbridge, S. J. Bame, J. T. Gosling, Energization of solar wind ions by reflection from the Earth's bow shock. *J. Geophys. Res.* **85**, 4689–4694 (1980).
10. H. Kucharek *et al.*, On the origin of field-aligned beams at the quasi-perpendicular bow shock: Multi-spacecraft observations by cluster. *Ann. Geophys.* **22**, 2301–2308 (2004).
11. C. F. Kennel, J. P. Edmiston, T. Hada, A quarter century of collisionless shock research. *Wash. DC Am. Geophys. Union Geophys. Monogr. Ser.* **34**, 1–36 (1985).
12. G. P. Zank, Y. Zhou, W. H. Matthaeus, W. K. M. Rice, The interaction of turbulence with shock waves: A basic model. *Phys. Fluids* **14**, 3766–3774 (2002).
13. J. Giacalone, M. Neugebauer, The energy spectrum of energetic particles downstream of turbulent collisionless shocks. *Acta Pathol. Jpn.* **673**, 629–636 (2008).
14. D. Trotta, L. Franci, D. Burgess, P. Hellinger, Fast acceleration of transrelativistic electrons in astrophysical turbulence. *Acta Pathol. Jpn.* **894**, 136 (2020).
15. J. R. Jokipii, Cosmic-ray propagation. I. Charged particles in a random magnetic field. *Acta Pathol. Jpn.* **146**, 480 (1966).
16. P. Dmitruk, W. H. Matthaeus, N. Seenu, Test particle energization by current sheets and nonuniform fields in magnetohydrodynamic turbulence. *Acta Pathol. Jpn.* **617**, 667–679 (2004).
17. J. F. Drake, M. Swisdak, H. Che, M. A. Shay, Electron acceleration from contracting magnetic islands during reconnection. *Nature* **443**, 553–556 (2006).
18. L. Comisso, L. Sironi, The interplay of magnetically dominated turbulence and magnetic reconnection in producing nonthermal particles. *Acta Pathol. Jpn.* **886**, 122 (2019).
19. S. Servidio, W. H. Matthaeus, M. A. Shay, P. A. Cassak, P. Dmitruk, Magnetic reconnection in two-dimensional magnetohydrodynamic turbulence. *Phys. Rev. Lett.* **102**, 115003 (2009).
20. F. Pecora, F. Pucci, G. Lapenta, D. Burgess, S. Servidio, Statistical analysis of ions in two-dimensional plasma turbulence. *Sol. Phys.* **294**, 114 (2019).
21. E. N. Parker, The passage of energetic charged particles through interplanetary space. *Planet. Space Sci.* **13**, 9–49 (1965).
22. T. L. Jackson, M. Y. Hussaini, H. S. Ribner, Interaction of turbulence with a detonation wave. *Phys. Fluid. A* **5**, 745–749 (1993).
23. J. Giacalone, The efficient acceleration of thermal protons by perpendicular shocks. *ApJ Lett.* **628**, L37–L40 (2005).
24. J. Giacalone, Particle acceleration at shocks moving through an irregular magnetic field. *Acta Pathol. Jpn.* **624**, 765–772 (2005).
25. F. Guo, J. Giacalone, The acceleration of electrons at collisionless shocks moving through a turbulent magnetic field. *Acta Pathol. Jpn.* **802**, 97 (2015).
26. D. Caprioli, A. Spitkovsky, Simulations of ion acceleration at non-relativistic shocks. II. Magnetic field amplification. *Acta Pathol. Jpn.* **794**, 46 (2014).
27. C. C. Haggerty, D. Caprioli, Kinetic simulations of cosmic-ray-modified shocks. I. Hydrodynamics. https://arxiv.org/abs/2008.12308 (27 August 2020).
28. S. Perri, S. Servidio, A. Vaivads, F. Valentini, Numerical study on the validity of the Taylor hypothesis in space plasmas. *ApJ Supp.* **231**, 4 (2017).
29. P. D. Mininni, A. Pouquet, Rotating helical turbulence. II. Intermittency, scale invariance, and structures. *Phys. Fluids* **22**, 035106 (2010).
30. D. Trotta, D. Burgess, Electron acceleration at quasi-perpendicular shocks in sub- and supercritical regimes: 2D and 3D simulations. *Mon. Not. R. Astron. Soc.* **482**, 1154–1162 (2019).
31. K. B. Quest, Simulations of high-Mach-number collisionless perpendicular shocks in astrophysical plasmas. *Phys. Rev. Lett.* **54**, 1872–1874 (1985).
32. J. A. le Roux, G. P. Zank, O. V. Khabarova, Self-consistent energetic particle acceleration by contracting and reconnecting small-scale flux ropes: The governing equations. *Acta Pathol. Jpn.* **864**, 158 (2018).
33. S. Servidio *et al.*, Explosive particle dispersion in plasma turbulence. *Phys. Rev. Lett.* **117**, 095101 (2016).
34. A. Kolmogorov, The local structure of turbulence in incompressible viscous fluid for very large Reynolds' numbers. *Akademiia Nauk SSSR Doklady* **30**, 301–305 (1941).
35. A. Greco, F. Valentini, S. Servidio, W. H. Matthaeus, Inhomogeneous kinetic effects related to intermittent magnetic discontinuities. *Phys. Rev. E* **86**, 066405 (2012).
36. A. Greco, W. H. Matthaeus, S. Servidio, P. Chuychai, P. Dmitruk, Statistical analysis of discontinuities in solar wind ACE data and comparison with intermittent MHD turbulence. *ApJ Lett.* **691**, L111–L114 (2009).
37. L. Sorriso-Valvo, V. Carbone, P. Veltri, G. Consolini, R. Bruno, Intermittency in the solar wind turbulence through probability distribution functions of fluctuations. *Geophys. Res. Lett.* **26**, 1801–1804 (1999).
38. L. J. Gleeson, The equations describing the cosmic-ray gas in the interplanetary region. *Planet. Space Sci.* **17**, 31–47 (1969).
39. J. R. Jokipii, Particle acceleration at a termination shock 1. Application to the solar wind and the anomalous component. *J. Geophys. Res.* **91**, 2929–2932 (1986).
40. G. P. Zank *et al.*, Diffusive shock acceleration and reconnection acceleration processes. *Acta Pathol. Jpn.* **814**, 137 (2015).
41. A. Leonard, Energy cascade in large-eddy simulations of turbulent fluid flows. *Adv. Geophys.* **18**, 237 (1974).
42. G. L. Eyink, Cascades and dissipative anomalies in nearly collisionless plasma turbulence. *Phys. Rev. X* **8**, 041020 (2018).
43. E. Camporeale, L. Sorriso-Valvo, F. Califano, A. Retinò, Coherent structures and spectral energy transfer in turbulent plasma: A space-filter approach. *Phys. Rev. Lett.* **120**, 125101 (2018).
44. M. Germano, U. Piomelli, P. Moin, W. H. Cabot, A dynamic subgrid-scale eddy viscosity model. *Phys. Fluid. A* **3**, 1760–1765 (1991).
45. Y. Yang *et al.*, Scale dependence of energy transfer in turbulent plasma. *Mon. Not. Roy. Astron. Soc.* **482**, 4933–4940 (2018).
46. J. R. Jokipii, Rate of energy gain and maximum energy in diffusive shock acceleration. *Acta Pathol. Jpn.* **313**, 842 (1987).
47. J. R. Jokipii, M. A. Lee, Compression acceleration in astrophysical plasmas and the production of f(v) vprop v $^{-5}$ spectra in the heliosphere. *Acta Pathol. Jpn.* **713**, 475–483 (2010).
48. L. R. Lyons, Pitch angle and energy diffusion coefficients from resonant interactions with ion-cyclotron and whistler waves. *J. Plasma Phys.* **12**, 417–432 (1974).
49. M. Lesieur, O. Metais, New trends in large-eddy simulations of turbulence. *Annu. Rev. Fluid Mech.* **28**, 45–82 (1996).
50. G. G. Howes, K. G. Klein, T. C. Li, Diagnosing collisionless energy transfer using field-particle correlations: Vlasov-Poisson plasmas. *J. Plasma Phys.* **83**, 705830102 (2017).
51. C. H. K. Chen, K. G. Klein, G. G. Howes, Evidence for electron Landau damping in space plasma turbulence. *Nat. Commun.* **10**, 740 (2019).
52. B. D. G. Chandran *et al.*, Stochastic heating, differential flow, and the alpha-to-proton temperature ratio in the solar wind. *Acta Pathol. Jpn.* **776**, 45 (2013).
53. D. Trotta, D. Burgess, G. Prete, S. Perri, G. Zimbardo, Particle transport in hybrid PIC shock simulations: A comparison of diagnostics. *Mon. Not. Roy. Astron. Soc.* **491**, 580–595 (2020).
54. E. Amato, P. Blasi, Cosmic ray transport in the galaxy: A review. *Adv. Space Res.* **62**, 2731–2749 (2018).
55. F. A. Aharonian, Gamma rays from supernova remnants. *Astropart. Phys.* **43**, 71–80 (2013).
56. S. Servidio *et al.*, Magnetospheric multiscale observation of plasma velocity-space cascade: Hermite representation and theory. *Phys. Rev. Lett.* **119**, 205101 (2017).
57. O. Pezzi *et al.*, Velocity-space cascade in magnetized plasmas: Numerical simulations. *Phys. Plasmas* **25**, 060704 (2018).

PHYSICS